JOM, Vol. 65, No. 12, 2013
DOI: 10.1007/s11837-013-0778-x

Thermal Recycling of Waelz Oxide Using Concentrated Solar Energy

N. TZOUGANATOS,[1] R. MATTER,[2] C. WIECKERT,[1]
J. ANTREKOWITSCH,[3] M. GAMROTH,[4] and A. STEINFELD[1,2,5]

1.—Solar Technology Laboratory, Paul Scherrer Institute, 5232 Villigen, Switzerland. 2.—Department of Mechanical and Process Engineering, ETH Zurich, 8092 Zurich, Switzerland. 3.—Department of Metallurgy, Montan University, 8700 Leoben, Austria. 4.—Befesa Steel Services GmbH, 47269 Duisburg, Germany. 5.—e-mail: aldo.steinfeld@ethz.ch

The dominating Zn recycling process is the so-called Waelz process. Waelz oxide (WOX), containing 55–65% Zn in oxidic form, is mainly derived from electric arc furnace dust produced during recycling of galvanized steel. After its wash treatment to separate off chlorides, WOX is used as feedstock along with ZnS concentrates for the electrolytic production of high-grade zinc. Novel and environmentally cleaner routes for the purification of WOX and the production of Zn are investigated using concentrated solar energy as the source of high-temperature process heat. The solar-driven clinkering of WOX and its carbothermal reduction were experimentally demonstrated using a 10 kW_{th} packed-bed solar reactor. Solar clinkering at above 1265°C reduced the amount of impurities below 0.1 wt.%. Solar carbothermal reduction using biocharcoal as reducing agent in the 1170–1320°C range yielded 90 wt.% Zn.

INTRODUCTION

The extensive application of zinc as an anticorrosion agent for steel, increasing global steel production and recycling, and the lack of zinc concentrates are main drivers for the development of zinc recycling technologies. Galvanized steel structures are scrapped after their operational life span and new steel is recovered in electric arc furnaces (EAFs). This energy-intensive process results in the concomitant generation of 15–25 kg of EAF dust per ton of steel. EAF dust consists mainly of Zn (18–35 wt.% as ZnO, ZnS, and $ZnCl_2$), Fe (30–40 wt.% as Fe and Fe oxides), as well as Ca and Si compounds. It is categorized as a hazardous solid waste material.[1,2] The majority of the EAF dust generated worldwide is disposed in hazardous waste storage and landfill sites, without taking advantage of the possibility of converting waste materials to valuable feedstock for processes in closed material cycles. High stabilization and disposal costs, limited storage space, and strict environmental regulations have, however, urged the need for increasing recycling of EAF dust by pyrometallurgical,[3–6] hydrometallurgical,[7–9] and chemical separation processes. More than 95% of the EAF dust recycling capacity is provided by pyrometallurgical processes, the dominating of which is the so-called Waelz process.[4,5] The use of high-temperature solar process heat for this purpose has been previously proposed and experimentally demonstrated.[10,11]

In the Waelz process, EAF dust is fed continuously into a rotary kiln along with a carbonaceous reducing agent and a slag-forming sand or lime. The kiln is slightly inclined for enabling residence times of 6–9 h. The charge is transformed at about 1200°C into the iron-rich Waelz slag (composed mainly of 35–45 wt.% Fe, 17–25 wt.% CaO, and 7–10 wt.% SiO_2) and Waelz oxide (WOX).[1] The latter is produced upon the volatilization of the nonferrous components of the charge, mainly Zn and Pb, during the carbothermal reduction and their subsequent oxidation in an air flow entering through the discharge end of the kiln. Under normal operating conditions, the process is autothermal. The crude WOX generated contains about 60–65% Zn, mainly in the form of ZnO. In addition, chlorides (3–7 wt.% Cl as NaCl, KCl, $CaCl_2$, $ZnCl_2$, $PbCl_2$, Pb(OH)Cl) and fluorides (0.05–0.2 wt.% F as NaF, KF, CaF_2) are accumulated. These compounds restrict the direct feeding of WOX to the primary Zn electrolytic production plant. Thus, the last unit of the Waelz process comprises washing for dehalogenation of

(Published online October 16, 2013)

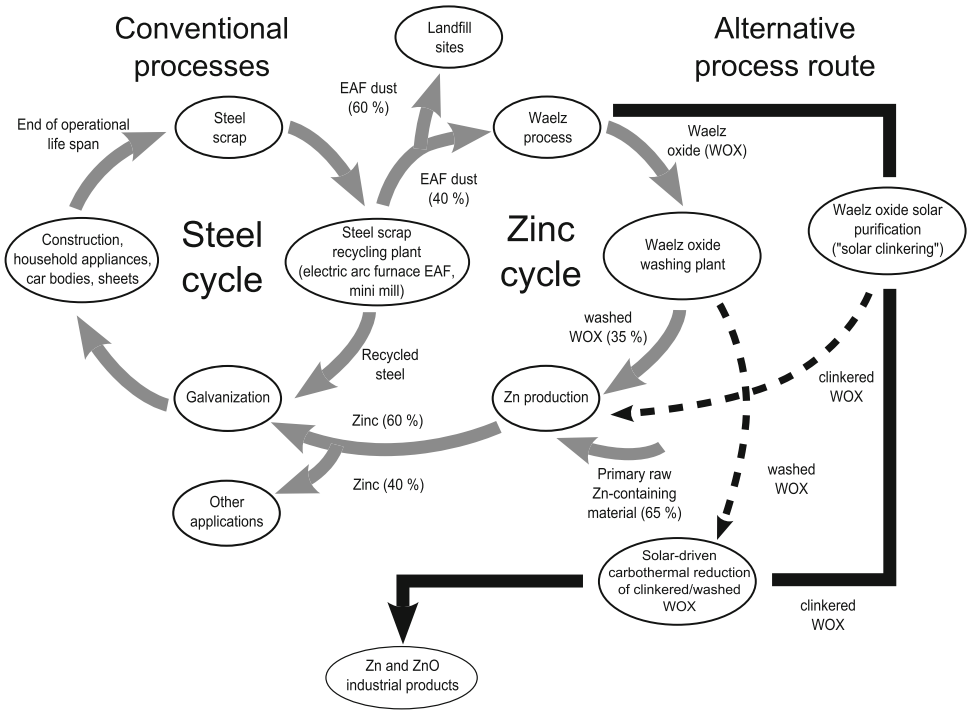

Fig. 1. Process flow diagram for the conventional steel and zinc industry and alternative routes using concentrated solar energy.

crude WOX. The end product, which constitutes a Zn concentrate (65–68 wt.% Zn), with chlorine and fluorine contents below 0.1 wt.% and 0.15 wt.%, respectively, is then obtained upon leaching of WOX.[12] Washed WOX enters the Zn cycle as an input feedstock together with ZnS from ores. The effluent, containing the dissolved components, can be either released as wastewater after its further treatment to comply with the water pollution emissions (e.g., precipitation of heavy metals and neutralization) or crystallized in an evaporation–crystallization unit.

In this article, alternative cleaner process routes for the purification of WOX and the carbothermal production of Zn are investigated using concentrated solar energy to drive the highly endothermic reactions, as depicted in Fig. 1. The first process considered is the solar-driven thermal purification of crude WOX via volatilization at temperatures in the range of 1000–1285°C—referred as "solar clinkering"—to yield clinkered WOX, which has higher Zn content than washed WOX (>80 wt.% ZnO) and can be used as feedstock for the carbothermal production of zinc. The second process considered is the solar-driven carbothermal reduction of clinkered WOX. Biomass is the preferred reducing agent for a CO_2-neutral process and for a high fraction of solar energy to be stored in Zn.[13] The simplified net reaction can be described by:

$$\mathrm{ZnO(s)} + \mathrm{C(s)} = \mathrm{Zn(g)} + \mathrm{CO} \qquad \Delta H^{\circ}_{298\mathrm{K}} = 239.9\ \mathrm{kJ\ mol^{-1}} \tag{1}$$

The predominant reaction route is via the solid–gas reaction[14]:

$$\mathrm{ZnO(s)} + \mathrm{CO} = \mathrm{Zn(g)} + \mathrm{CO_2} \qquad \Delta H^{\circ}_{298\mathrm{K}} = 67.5\ \mathrm{kJ\ mol^{-1}} \tag{2}$$

where CO is formed by the Boudouard equilibrium:

$$\mathrm{CO_2} + \mathrm{C(s)} = 2\ \mathrm{CO} \quad \Delta H^{\circ}_{298\mathrm{K}} = 172.4\ \mathrm{kJ\ mol^{-1}}. \tag{3}$$

Besides its wide industrial application as material commodity, Zn can be used as a fuel in Zn-air batteries[15,16] or reacted with H_2O and CO_2 to form high-purity H_2[17–21] and CO,[22] which are precursors for synthetic liquid fuels.[23,24] Alternatively, Zn can be oxidized at the solar reactor exit for the production of high-purity ZnO. The technical feasibility of a packed-bed solar reactor is experimentally investigated for performing both processes: the solar clinkering of WOX and the solar carbothermal reduction of clinkered WOX. In the solar clinkering experiments, the focus is in elucidating the influence of temperature and irradiation time on the composition of clinkered WOX. In the carbothermal reduction experiments, the main focus lies on the Zn production rate and Zn content in the condensed product.

EXPERIMENTAL

Solar Concentrating System

Experimentation was carried out at Paul Scherrer Institute's high-flux solar simulator (HFSS).[25] This

research facility comprises an array of ten high-pressure Xe arcs close coupled with ellipsoidal specular reflectors and provides up to 50 kW_{th} of thermal radiative power at peak radiative fluxes of 11,000 suns (1 sun = 1 kW/m^2). Thus, solar receivers and reactors can be tested under the same radiative heat transfer characteristics of highly concentrating solar systems. Power flux intensities can be regulated by the number of arcs in operation, the relative position of the test target to the focal plane, and the Venetian blind-type shutter located between the arcs and the solar reactor. The input solar radiative power and flux distributions are measured optically with a calibrated charge-coupled device (CCD) camera on an Al_2O_3-plasma coated Lambertian target with an accuracy of 10%. A water-cooled, Al-polished 45°-deflection mirror is used for redirecting the incoming horizontal beam into a vertical beam entering a three-dimensional compound parabolic concentrator (CPC).[26] The CPC, of 80 mm-diameter entrance and 65 mm-diameter exit, is incorporated at the reactor's aperture to boost the incoming radiation flux intensity and decrease reradiation losses through a smaller aperture size.

Solar Reactor

The solar reactor configuration is shown schematically in Fig. 2. It is specifically designed for beam-down operation as obtained through a Cassegrain optical configuration that makes use of a hyperbolic reflector at the top of a solar tower to redirect sunlight collected by a heliostat field to a receiver located at ground level.[27] It consists of two cavities in series, separated by a 170 mm-diameter 5 mm-thick SiC-coated graphite plate. The upper cavity is subjected to concentrated solar irradiation entering through a 65 mm-diameter circular aperture with a 2 mm-thick quartz window. The lower cavity is an octagonal, 135 mm-diameter, 170 mm-high enclosure that serves as the reaction chamber and contains a packed bed of solid reactants. With this arrangement, concentrated solar radiation is efficiently absorbed by the upper cavity, reradiated by the hot separation plate toward the lower cavity, and absorbed by the top of the packed bed. An inert carrier gas enters the upper cavity, cools the window, and flows through small gaps around the separation plate into the lower cavity to prevent reaction gas from reaching the quartz window. The lower cavity is also flushed with an inert carrier gas entering the reactor below the separation plate. The gaseous products are swept out through a 50 mm-diameter outlet port located on the lateral walls of the lower cavity, above the packed bed. The walls of the lower cavity are lined with 8 mm-thick SiC plates to prevent the diffusion of condensable gaseous products into the insulation material. Both cavities are well insulated to reduce heat conduction losses. The two-cavity reactor configuration enables the protection of the quartz window against condensable gases and particle depositions by the separation plate, and thus it eliminates a major problem encountered in windowed reactors. Generic design guidelines for maximization of the thermal efficiency of the two-cavity reactor configuration are provided based on radiation heat transfer analyses.[28,29]

Experimental Setup

A flow diagram of the experimental setup is shown in Fig. 3. Inert gas (N_2) mass flow rates are controlled by Bronkhorst flow meters (EL-flow

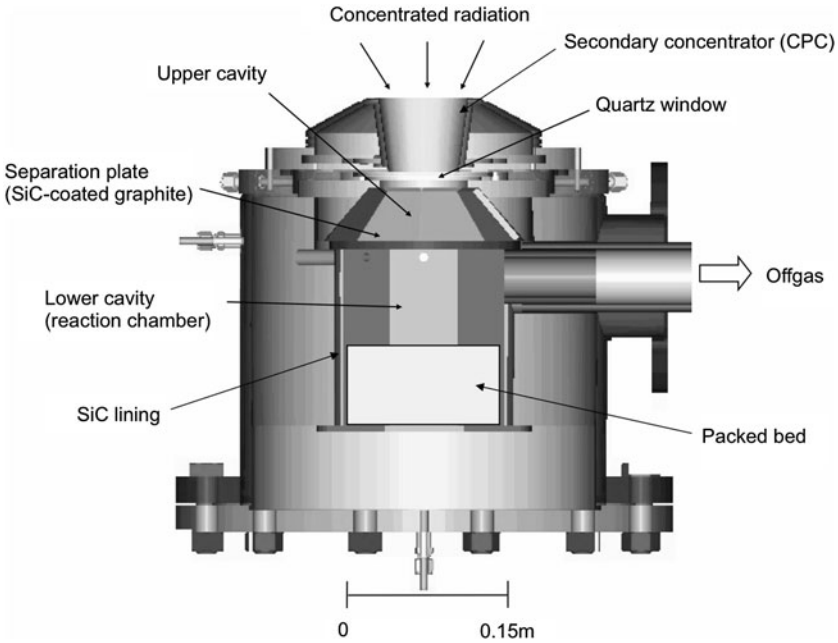

Fig. 2. Schematic of the 10 kW_{th} packed-bed solar reactor.

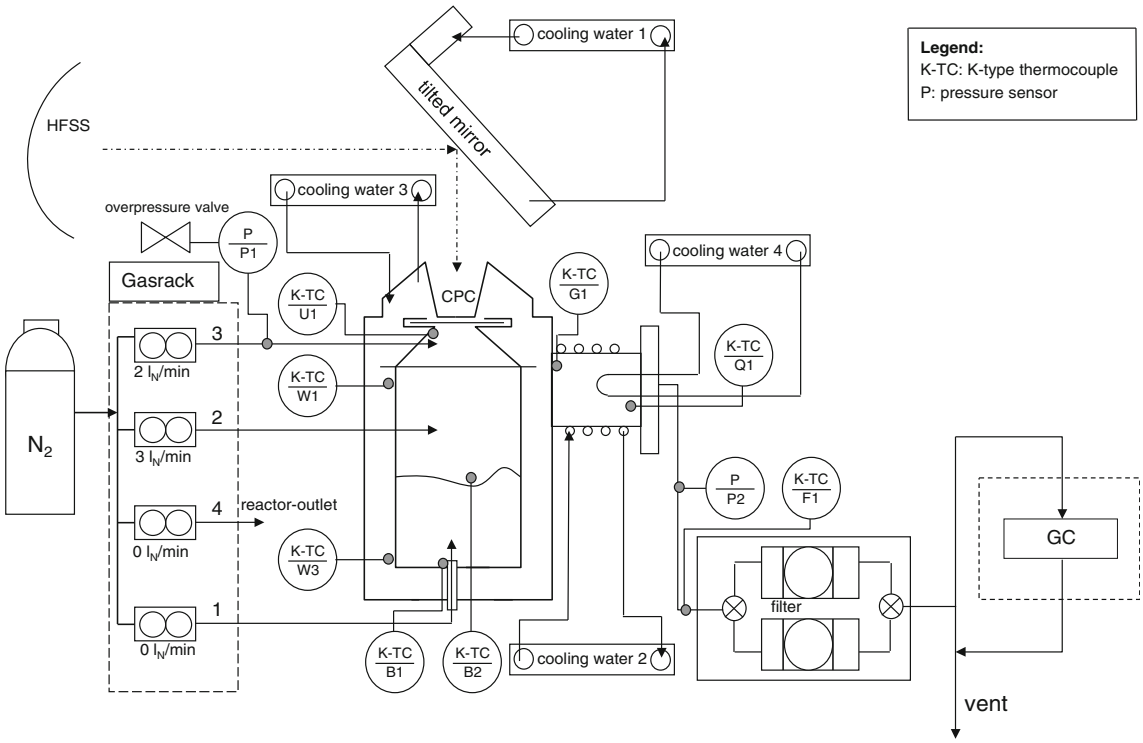

Fig. 3. Flow diagram of the experimental setup comprising the solar concentrating system, the solar reactor, the off-gas system, and the diagnostic instrumentation.

series). Two and three L_N min^{-1} (L_N means liters at normal conditions; mass flow rates are calculated at 273 K and 1 bar) enter the upper and lower cavity, respectively. After exiting the reactor, the carrier gas and the gaseous products flow through a water-cooled condenser where part of the condensable products deposit before passing through a filtering system. The composition of the noncondensable product gases behind the filter is analyzed online by gas chromatography (Micro GC M200, 0.01 Hz sampling rate; Agilent Technologies, Santa Clara, CA). All experiments were performed at slightly above ambient pressure, with relative pressures of ~5–10 mbar. The pressure is monitored online in the upper cavity of the reactor (P1) and upstream of the filter unit (P2). A pressure relief valve opening at a pressure of 150 mbar prevents damage of the quartz window in the case of clogging of the off-gas system. Packed-bed, reaction chamber walls, and off-gas temperatures are measured at eight locations by type-K thermocouples. Temperatures at the top (T_{B2}) and bottom of the packed bed (T_{B1}) provide the temperature gradient across the bed. For the carbothermal reduction, $T_{B2} - T_{B1}$ indicates the remaining unreacted material and ash. The temperatures of the separation plate (T_{U1}) and of the inner SiC lining approximately 8 mm below the separation plate (T_{W1}) are representative for the upper and lower cavity, respectively.

Materials

The crude and washed WOX used for the experiments originated from the Waelz kiln at Befesa Freiberg, Germany. Washed WOX was derived in the washing plant upon a three-step leaching of crude WOX. The elemental composition in % (w/w) of a dried sample is listed in Table I.

For crude WOX, Zn, Pb, and Fe were present primarily in their oxidized state with ZnO being the main constituent in the range 71–77 wt.%,[30] whereas the remaining components were in the form of chlorides ($ZnCl_2$, $PbCl_2$, NaCl, and KCl) and sulfates. For washed WOX, the ZnO content varied in the range of 83–87 wt.%. The pronounced decrease in the K, Na, and Cl contents in washed WOX is attributed to the depletion of chlorine by washing, which generates Zn-, Pb-, and Fe-enriched mixtures. The water content of the crude and washed WOX determined by drying at 105°C for 24 h was 1.1 wt.% and 12.6 wt.%, respectively. To ensure well-characterized properties and precise ZnO:C molar ratios in the starting reacting mixture, commercial ZnO (Alfa Aesar, Ward Hill, MA; 011558, purity: 99.0% min, mean particle size 44 μm) was used as feedstock in several carbothermal reduction runs for comparison with runs using crude, washed, and clinkered WOX as feedstock. Beech charcoal gravel (proFagus, Bodenfelde, Germany; carbon content 83 wt.%, particle size 0.5–1.0 mm) was used

Table I. Elemental composition of crude and washed WOX (dry basis)

Element	Crude WOX (wt.%)	Washed WOX (wt.%)
Zn	60.05	68.30
Pb	3.64	5.17
Cl	5.57	0.43
K	3.49	0.09
Na	1.62	0.26
Fe	1.64	2.64
C	1.33	1.39
S	0.58	0.16
F	0.12	0.20

Oxygen is complementary to 100%.

Table II. Chemical composition of beech charcoal ash

Component	Wt.%
CaO	44.81
SiO_2	20.00
MgO	14.44
K_2O	4.36
SO_3	3.52
MnO	3.01
Al_2O_3	2.43
FeO	2.20
TiO_2	1.29
Na_2O	0.94
Zn	0.10
Cu	0.05
Ni	0.05
Cl	0.02

as reducing agent because it is a widely available biogenic material suitable for the CO_2-neutral solar carbothermal reduction of ZnO.[31] It contained 83 wt.% C, 9.74 wt.% O, 3.02 wt.% H, 0.38 wt.% N, 0.01 wt.% S, and 2.2 wt.% ash. The ash composition is listed in Table II. Softening and fusion occur at 1210°C and 1415°C, respectively.[31]

The composition of raw materials was analyzed by x-ray powder diffraction (XRD; Phillips, Almelo, the Netherlands; XPert MPD/DY636, Cu Kα, λ = 1.540598 Å, 2θ = 20°–90°, step size 0.05°, scan speed 0.01°/s) and their morphology was examined by scanning electron microscopy (SEM, SmartSEM, Carl Zeiss Supra 55VP; Carl Zeiss, Oberkochen, Germany). As expected, ZnO, PbO, Fe_2O_3, NaCl and KCl were the dominating phases in crude WOX. No NaCl and KCl were detected for the washed WOX. The SEM pictures of the crude and washed WOX, commercial ZnO, and beech charcoal are shown in Fig. 4. The commercial ZnO and the majority of the crude and washed WOX particles exhibited a wurtzite crystal structure: a hexagonal lattice consisting of two interconnecting sublattices of Zn^{2+} and O^{2-}, which allow the tetrahedral coordination of Zn and O atoms. All ZnO sources comprised highly agglomerated grains with negligible intraparticle porosity, indicating that the porosity can be attributed mainly to the interparticle void spaces. Crude and washed WOX also contained fine needles and sponge-like structures. Beech charcoal was highly branched and contained tubular pores.

Experimental Procedure

For the solar clinkering experiments, batches of crude WOX were loaded on a crucible made of heat-resistant austenitic stainless steel (Böhler H525, 1.4841; Böhler, Kapfenberg, Germany) resulting in a ~40 mm-thick porous bed. The upper and lower cavities were initially flushed with N_2. After ensuring O_2 concentration below 300 ppm, the HFSS was ignited and the shutter opening was increased stepwise at a 10% increment every 3 min, allowing the gradual heating of the packed bed to the desired temperature T_{B1}. This temperature was maintained constant for different time intervals (0, 15, 30, and 75 min) depending on the goal of each experiment. At the end, the shutter was closed and the HFSS was switched off. The carrier gas flow was maintained until the cavity cooled down. The same procedure was followed for the carbothermal reduction experiments. ZnO:C molar ratios of reactants ranged between 1:0.8 and 1:1.25. The values listed in Table I were used for the calculation of the molar ratios when crude or washed WOX were used as feedstock. The initial packed bed height was ~40 mm. T_{B1} was kept constant until the CO and CO_2 concentrations approached zero, indicating that the reaction neared completion. The Zn production rate was calculated from the oxygen balance in CO and CO_2. This calculation slightly overestimated the amount of Zn produced because it did not account for the oxygen content in charcoal and impurity oxides (PbO, Fe_2O_3, etc.) present in crude, washed, or clinkered WOX, a fraction of which may end up in CO or CO_2 as well. Products were analyzed for their Zn, Pb, Cl, F, K, Na, and Fe content by elemental analysis, for their phase composition by XRD, and for their morphology by SEM.

RESULTS AND DISCUSSION

Solar Clinkering

Fifteen experimental runs were carried out with the solar radiative power input in the range 4.1–4.85 kW_{th}. Under approximately steady-state conditions, the packed-bed top (T_{B2}) and bottom (T_{B1}) temperatures reached 1050–1310°C and 1000–1285°C, respectively. A representative run with 470 g of crude WOX is shown in Fig. 5. After the stepwise increase of the radiative power input to 3.2 kW_{th} within the first 18 min, the upper cavity temperature (T_{U1}) increased to 840°C and the one at the top of the packed bed (T_{B2}) to 420°C. Small

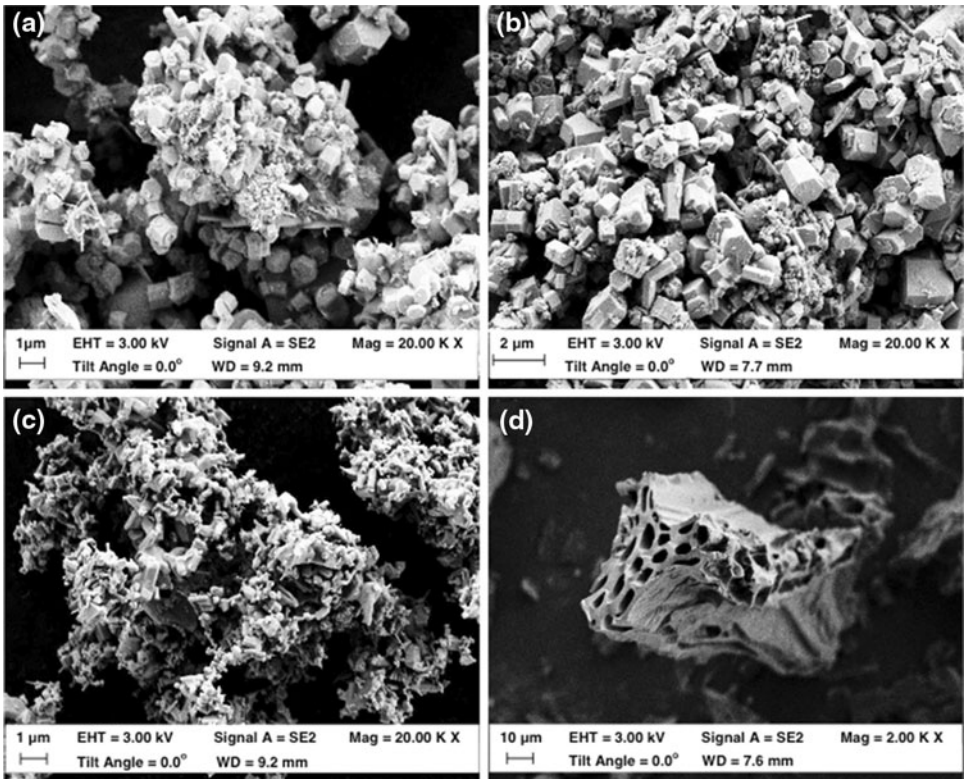

Fig. 4. SEM pictures of: (a) crude WOX, (b) washed WOX, (c) commercial ZnO, and (d) beech charcoal.

amounts of CO_2 were attributed to residual oxygen. The full opening of the shutter after 27 min was immediately followed by the formation of higher CO_2 amounts. After 40 min, the reaction proceeded at higher rates once T_{B2} and T_{B1} reached 965°C and 360°C, respectively. The temperature gradient across the packed bed decreased with time due to the shrinkage of the bed; a temperature difference of ~90°C (T_{B2} = 1310°C and T_{B1} = 1220°C) was observed at steady-state conditions. The gas flow rate of CO_2 reached a maximum of 0.012 mol/min after 55 min, while CO and H_2 were also detected in the off-gas flow. CO became the predominant component of the off-gas at higher temperatures, consistent with the Boudouard equilibrium (Eq. 3). T_{B1} stabilized after 100 min and the evolution of CO and CO_2 ceased, indicating the consumption of the carbon contained in the crude WOX. The desired T_{B1} of 1220°C was reached after 130 min and maintained during 30 min before turning off the HFSS. The clinkered WOX collected from the crucible contained 68.1 wt.% Zn, 0.92 wt.% Cl, and 0.79 wt.% Pb. Other elements present in lower percentage were Fe and Ca. The effectiveness of solar clinkering in terms of the Zn content was comparable to the one acquired by the industrial washing process (see washed WOX in Table I). The decrease of Pb content was even better. ZnO, Fe_2O_3, MnO, PbO, and KCl were detected by XRD analysis, while no NaCl peaks were found. A representative SEM picture of clinkered WOX that underwent partial melting is

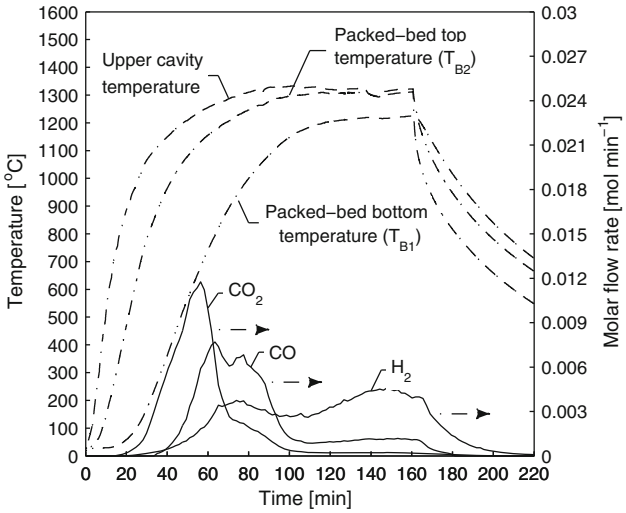

Fig. 5. Solar reactor temperatures and molar flow rates of CO, CO_2, and H_2 during a representative solar clinkering experiment with 470 g of crude WOX.

shown in Fig. 6. Condensed by-products were deposited on the condenser walls, the cooling finger, the outlet pipes, and the filter. XRD analysis revealed the presence of ZnO, Zn, NaCl, KCl, PbO, and Pb. Zn was presumably formed by the reduction of ZnO with the small amount of carbon contained in crude WOX (~1.3 wt.%). Films of ZnO were formed on the Zn surface upon exposure to air.

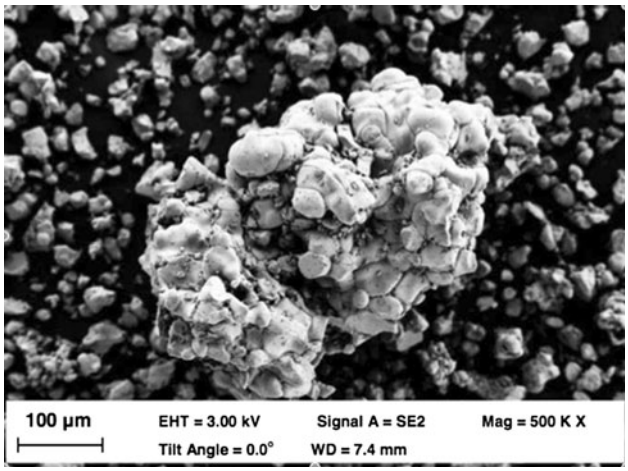

Fig. 6. SEM of solar-clinkered WOX.

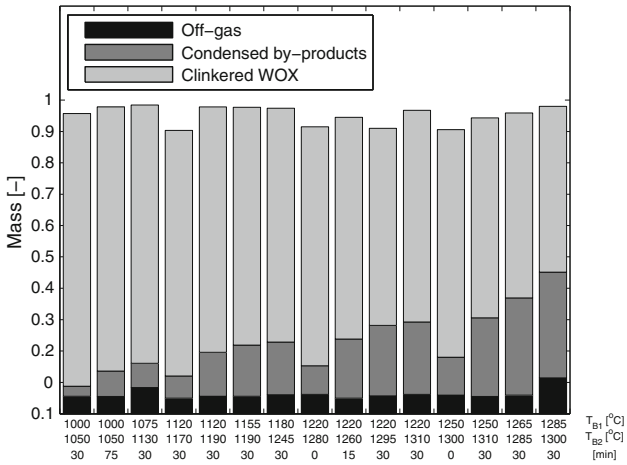

Fig. 7. Normalized mass balance for the solar clinkering experiments. The nominal temperatures at the bottom (T_{B1}) and top (T_{B2}) of the packed bed and the irradiation time period at this temperature level are indicated in the *x* axis.

NaCl, KCl, and PbO evaporated at the temperatures investigated, thus decreasing the Cl and Pb content of the processed crude WOX. The formation of Pb can be attributed to the reduction of PbO with CO, either at the surface of the off-gas system components or during condensation in the aerosol.

The normalized mass balance is shown in Fig. 7 for all 15 solar clinkering experiments. Also indicated are the nominal temperatures at the bottom (T_{B1}) and top (T_{B2}) of the packed bed and the irradiation time period at this temperature level. The mass balance is satisfactorily closed for most experiments. Deviations from 100% are partially attributed to the discrete measurements of the gas composition (0.01 Hz sampling rate). CO, CO_2, and H_2 accounted for ~5–11% of the mass and were linked to the amount of carbon in crude WOX

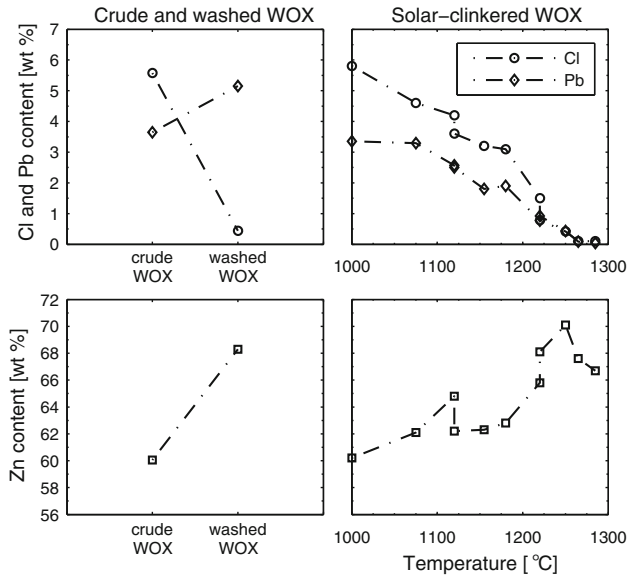

Fig. 8. Zn, Cl, and Pb content of crude, washed, and solar-clinkered WOX.

Table III. Boiling points of Cl and Pb compounds

Element/compound	Boiling point (°C)
$ZnCl_2$	732
$PbCl_2$	950
KCl	1413
NaCl	1465
PbO	1470
Pb	1749

(~1.3 wt.%). Temperature had a profound effect on the amount of condensed by-products because of the nonlinear dependence of the vapor pressure with temperature, which favors vaporization from crude WOX. Larger amounts of condensed by-products were detected with increasing irradiation times, indicating that evaporation was not completed for the short tests. A comparison of the compositions of crude, washed, and solar-clinkered WOX with respect to the Zn, Cl, and Pb content is provided in Fig. 8. In this figure, the irradiation time period for solar clinkering was 30 min. A notable decrease of Cl and Pb with increasing temperature was observed, which was accompanied by an increase in the Zn content. As $ZnCl_2$ and $PbCl_2$ exerted higher vapor pressures compared to other Cl and Pb compounds (see Table III), they were vaporized at lower temperatures. The volatilization of KCl, NaCl, PbO, and Pb was favored with increasing temperature, leading to further purification of crude WOX. A Cl content of 0.42 wt.%, comparable to that of washed WOX, was reached after 30 min irradiation at T_{B1} = 1250°C. At T_{B1} > 1265°C, the Cl content

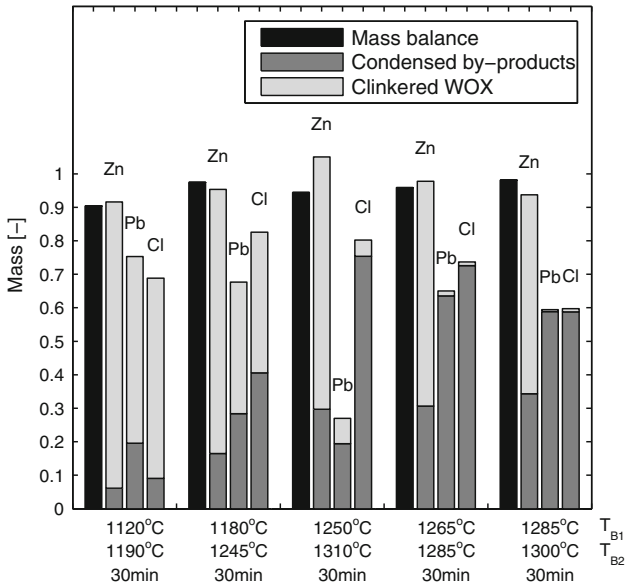

Fig. 9. Normalized mass and elemental (Zn, Pb, and Cl) balances for five selected solar clinkering runs. The nominal temperatures at the bottom (T_{B1}) and top (T_{B2}) of the packed bed and the irradiation time period at this temperature level are indicated in the *x* axis.

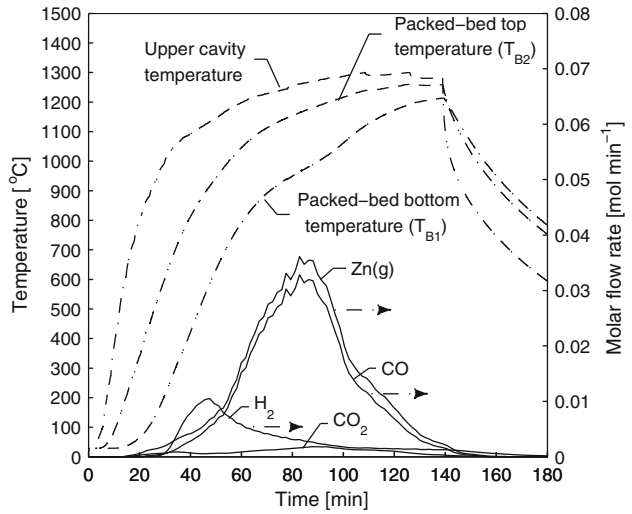

Fig. 10. Solar reactor temperatures and molar flow rates of Zn, CO, CO_2, and H_2 during a representative experimental run for the solar-driven carbothermal reduction of clinkered WOX, using 240 g of reactants with a ZnO:C molar ratio of 1:0.86.

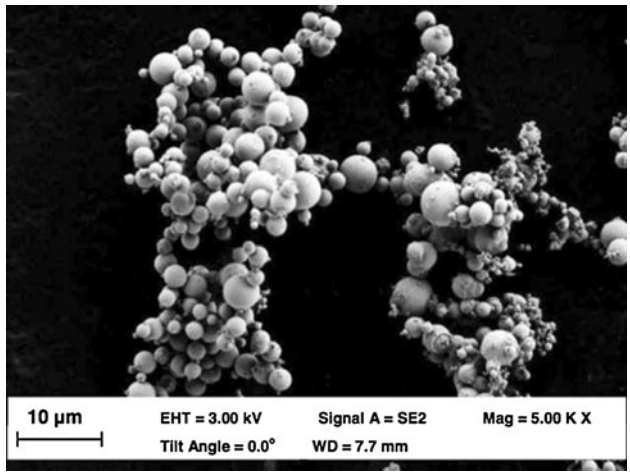

Fig. 11. SEM of condensed products from the solar carbothermal reduction.

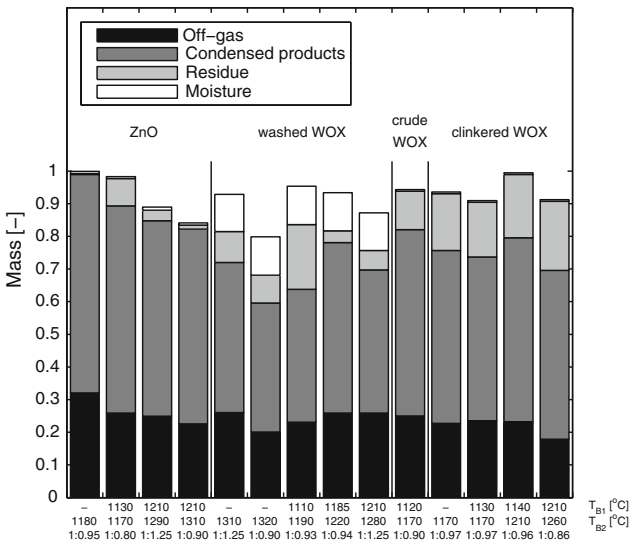

Fig. 12. Normalized mass balance of the solar carbothermal reduction experiments with different feedstock. The nominal temperatures at the bottom (T_{B1}) and top (T_{B2}) of the packed bed and the ZnO:C molar ratio are indicated in the *x* axis.

further decreased below 0.1%. In contrast to the conventional WOX washing process, very low residual Pb contents of 0.09 wt.% and 0.04 wt.% were obtained by solar clinkering at T_{B1} = 1265°C and 1285°C, respectively. This effective purification is of particular importance because it enables the direct neutralization of the product in the Jarosite step of the primary Zn production cycle[32] without the need to pass it through the roaster. The clinkered WOX and condensed by-products were analyzed for their Zn, Cl, and Pb content. The normalized mass and elemental balances are shown in Fig. 9 for five selected solar clinkering experimental runs at T_{B1} = 1120°C, 1180°C, 1250°C, 1265°C, and 1285°C. Also indicated are the nominal temperatures at the bottom (T_{B1}) and top (T_{B2}) of the packed bed and the irradiation time period at this temperature level. Satisfactory closing of the mass balance for Zn was accomplished. Diffusion of gaseous products into the insulation material presumably accounted for the missing Cl and Pb, as well as molten Pb accumulated at the bottom of the crucible. An error source of the analysis was the inhomogeneous character of the products, especially for Pb as its accurate content determination in the

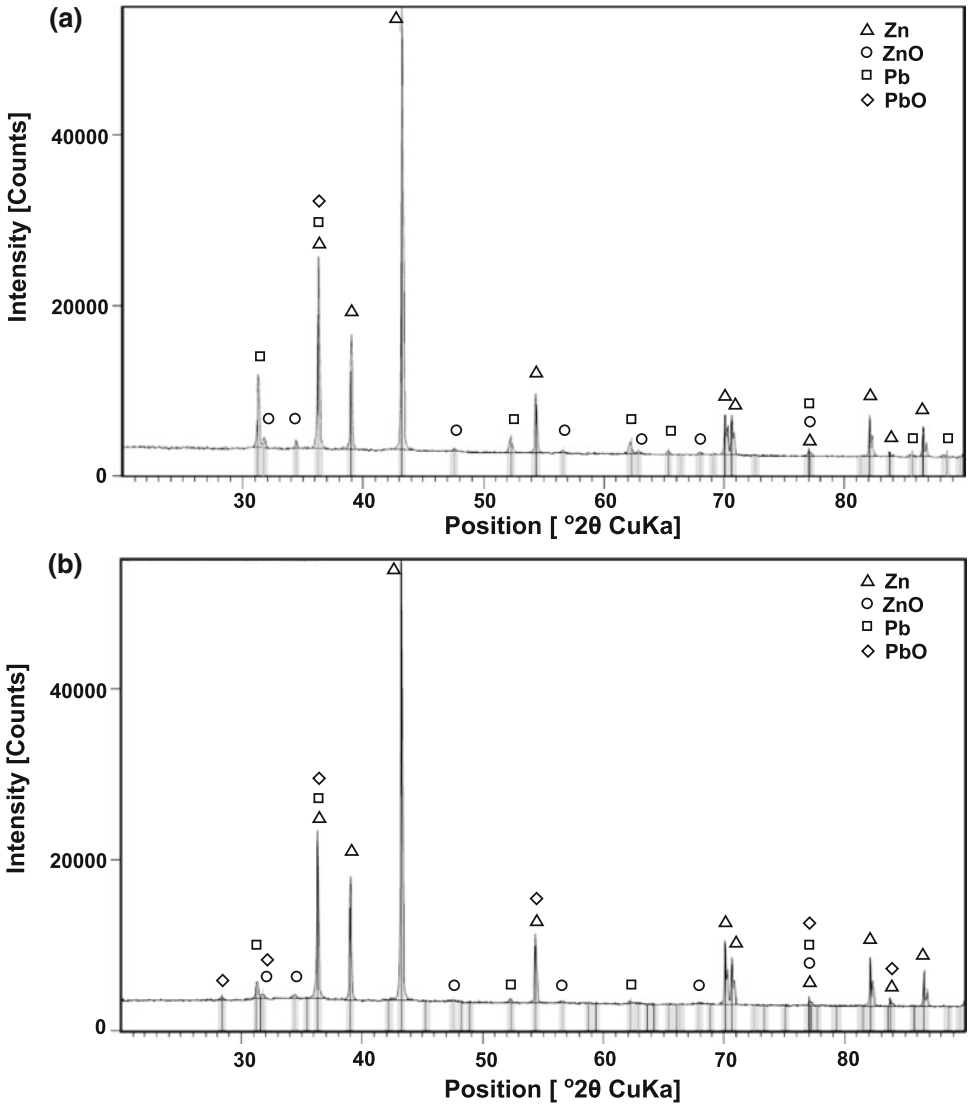

Fig. 13. XRD pattern of the condensed products for a representative run with (a) washed WOX (ZnO:C = 1:1.25, 1280°C) and (b) solar-clinkered WOX (30 min at T_{B1} = 1250°C, ZnO:C = 1:0.86, 1260°C).

clinkered WOX is difficult due to the occurrence of molten PbO and Pb phases.

Solar Carbothermal Reduction

A series of 14 experimental runs with ZnO:C molar ratios between 1:0.8 and 1:1.25 was carried out using crude, washed, and solar-clinkered WOX and commercial ZnO. Temperatures in the range of 1110–1210°C and 1170–1320°C were reached at approximately steady state at the bottom (T_{B1}) and top (T_{B2}) of the packed bed, respectively. A representative run with clinkered WOX and a ZnO:C molar ratio of 1:0.86 is shown in Fig. 10. After the first 20 min, T_{B2} = 340°C and T_{B1} = 65°C, and the evaporation and decomposition of volatiles occurred along with the evolution of small amounts of CO_2 and H_2. H_2 reached its concentration peak about 20 min later. The formation of CO started at T_{B2} = 480°C. The carbothermal reduction proceeded at high rates above 900°C as evidenced by the strong increase of the CO molar flow rate, which peaked at 0.033 mol/min after 83 min. This is consistent with the change in the slope of T_{B1} and the subsequent decrease of the temperature gradient across the bed. CO_2 represented only a small fraction of the gaseous product, indicative of its consumption via the Boudouard equilibrium (Eq. 3). The Zn production rate reached a maximum of 0.036 mol/min. T_{B2} stabilized at 1260°C and CO evolution decreased as the reaction neared completion. Toward the end of the experimental run, the small temperature difference between T_{B1} and T_{B2} (~50°C), along with the low gas evolution, indicated complete conversion of the reactants. A visual examination of the residue revealed the presence of unreacted charcoal. Solid products were collected from the condenser, outlet pipes, and filter. The

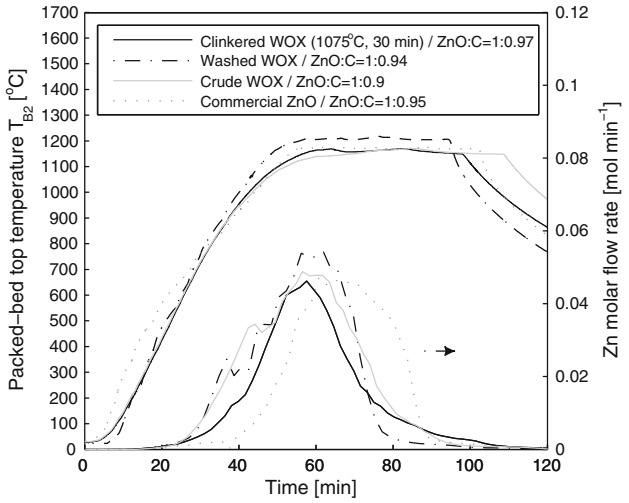

Fig. 14. Variation of the packed-bed top temperature and Zn production rate during the carbothermal reduction of crude, washed, and solar-clinkered WOX, and commercial ZnO.

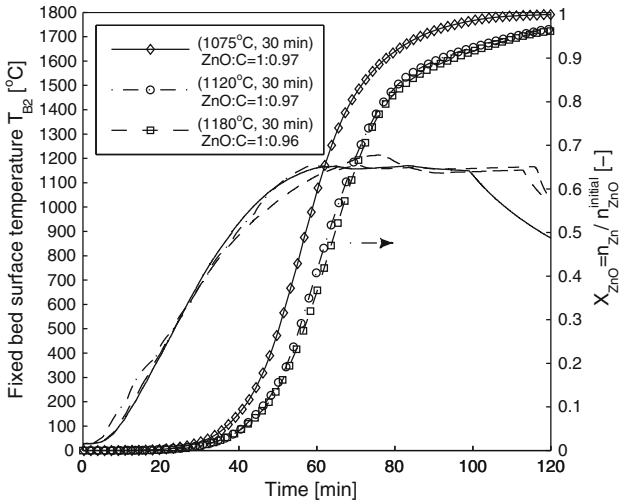

Fig. 15. Variation of temperature and chemical conversion as a function of time during the solar carbothermal reduction of three solar-clinkered WOX samples that were purified at T_{B1} = 1075°C, 1120°C, and 1180°C during 30 min.

SEM picture of Fig. 11 shows round agglomerated particles formed upon condensation and coalescence of Zn vapor at short residence times.

The normalized mass balance is shown in Fig. 12 for all 14 solar carbothermal experiments. Also indicated are the nominal temperatures at the bottom (T_{B1}) and top (T_{B2}) of the packed bed and the ZnO:C molar ratio. Off-gas accounts for ~18–32% of the initial mass, while the remainder was collected in the form of condensed products and reaction residue. Diffusion of condensable gas products into the insulation was partly responsible for the unclosed mass balance. This was corroborated by comparing of the total amount of Zn recovered in the off-gas to that calculated by integration of the production rate based on CO and CO_2 evolution over time. Typically, 60–80% of the ZnO reduced (based on the integration of CO and CO_2 evolved) could be recovered in the off-gas system as pure metallic Zn. However, as previously indicated, the calculation does not account for oxygen content in the reducing agent and feedstock's impurities. Condensed products from the experimental runs with washed WOX contained Zn in the range 85.2–92.4 wt.%, Pb in the range 3.4–3.8 wt.%, and Cl in the range 0.26–1.35 wt.%. An XRD analysis, shown in Fig. 13, revealed the presence of Zn, ZnO, and Pb for all ZnO sources, apart from commercial ZnO that showed no Pb as expected. With solar-clinkered WOX as a reactant, the intensity of the Pb diffraction peaks was significantly lower, indicating a higher purity of Zn. This was expected because the Pb content was reduced to much lower levels by solar clinkering compared to industrial washing. Pb resulted either from PbO vaporization and reduction with CO or directly from the carbothermal reduction of PbO.

The variation of the Zn production rate for the carbothermal reduction of the various ZnO feedstock—namely crude, washed, and solar-clinkered WOX, and for commercial ZnO—is shown in Fig. 14 for ZnO:C molar ratios in the range of 1:0.9–1:0.97. Both crude and washed WOX yielded faster reduction rates compared to solar-clinkered WOX and commercial ZnO. This is attributed to the inherently different morphology and properties of the various ZnO sources, affecting heat/mass transfer and intrinsic kinetics. The solar-clinkered WOX exhibited a lower specific surface area available for the solid–gas reaction (Eq. 2) due to partial sintering and melting. Note that the content of oxides other than ZnO (mainly PbO) in the crude and washed WOX resulted in an overestimation of the CO and CO_2 evolved from the carbothermal reduction of ZnO by up to 15% and 19%, respectively, as calculated from the asymptotic conversions. In terms of the maximum reduction rates, crude, washed, solar-clinkered WOX, and commercial ZnO yielded similar values to each other.

The effect of the heat treatment temperature during solar clinkering of crude WOX on the Zn production rate during the carbothermal reduction was explored with three solar-clinkered WOX samples that were purified at different temperatures, namely at T_{B1} = 1075°C, 1120°C, and 1180°C during 30 min. The variation of temperature and chemical conversion as a function of time during the carbothermal reduction of these three samples is shown in Fig. 15. Comparable asymptotic conversions were obtained for all samples. Slower rates were expected at higher clinkering temperatures because of the decrease of the specific surface area due to partial sintering/melting, but this effect was not observed for the temperatures considered.

CONCLUSIONS

Solar clinkering using concentrated solar energy was proposed as an alternative cleaner route to the

purification of WOX and experimentally demonstrated using a 10 kW_{th} packed-bed solar reactor. Cl and Pb contents lower than those of washed WOX (<0.1 wt.%) were attained by solar clinkering of crude WOX at elevated temperatures ($T_{B1} > 1265$°C). Depletion of Pb and its compounds represented a major advantage of the proposed solar-driven process vis-à-vis the industrial washing process and led to higher ZnO contents ($\sim$88 wt.%) in the product. The solar-driven production of Zn via the carbothermal reduction of clinkered, washed, and crude WOX was experimentally demonstrated using the same packed-bed solar reactor. Beech charcoal was used as reducing agent for a CO_2-neutral carbothermal process. Zn contents of about 90 wt.% were obtained in the condensed products. Incorporation of continuous or semicontinuous feeding of reactants and removal of products can improve product yield and thermal efficiency.

REFERENCES

1. V. Popovici (Paper presented at the 5th Global Slag Conference, Brussels, 23–24 November 2009).
2. T. Sofilic, A. Rastovcan-Mioc, S. Cerjan-Stefanovic, V. Novosel-Radovic, and M. Jenko, *J. Hazard. Mater.* 109, 59 (2004).
3. A.J. Xu, Q.X. Yang, B. Gustafsson, F. Wang, J.L. Li, and B. Bjorkman, *J. Iron. Steel Res. Int.* 17, 132 (2010).
4. J. Ruetten, *SEAISI Q. J.* 35, 13 (2006).
5. N.L. Piret, *World Metall. Erzmet.* 65, 306 (2012).
6. M.H. Morcali, O. Yucel, A. Aydin, and B. Derin, *J. Min. Metall. Sect. B* 48, 173 (2012).
7. N. Leclerc, E. Meux, and J.M. Lecuire, *J. Hazard. Mater.* 91, 257 (2002).
8. C. Caravaca, A. Cobo, and F.J. Alguacil, *Resour. Conserv. Recycl.* 10, 35 (1994).
9. J. Antrekowitsch and H. Antrekowitsch, *JOM* 53, 26 (2001).
10. B. Schaffner, W. Hoffelner, H.Y. Sun, and A. Steinfeld, *Environ. Sci. Technol.* 34, 4177 (2000).
11. B. Schaffner, A. Meier, D. Wuillemin, W. Hoffelner, and A. Steinfeld, *Environ. Sci. Technol.* 37, 165 (2003).
12. N. Menad, J.N. Ayala, F. Garcia-Carcedo, E. Ruiz-Ayucar, and A. Hernandez, *Waste Manag.* 23, 483 (2003).
13. C. Wieckert and A. Steinfeld, *J. Sol. Energy-Trans. ASME* 124, 55 (2002).
14. C.E. Guger and F.S. Manning, *Metall. Trans.* 2, 3083 (1971).
15. K.F. Blurton and A.F. Sammells, *J. Power Sources* 4, 263 (1979).
16. J.R. Goldstein and B. Koretz (Paper presented at Energy Environment Economics: 28th Intersociety Energy Conversion Engineering Conference Proceedings (Iecec-93), 1993), pp. 279–284.
17. K. Wegner, H. Ly, R. Weiss, S. Pratsinis, and A. Steinfeld, *Int. J. Hydrogen Energy* 31, 55 (2006).
18. R. Weiss, H. Ly, K. Wegner, S. Pratsinis, and A. Steinfeld, *AIChE J.* 51, 1966 (2005).
19. A. Steinfeld, *Sol. Energy* 78, 603 (2005).
20. A. Berman and M. Epstein, *Int. J. Hydrogen Energy* 25, 957 (2000).
21. E. Bilgen, M. Ducarroir, M. Foex, F. Sibieude, and F. Trombe, *Int. J. Hydrogen Energy* 2, 251 (1977).
22. P.G. Loutzenhiser, M.E. Galvez, I. Hischier, A. Stamatiou, A. Frei, and A. Steinfeld, *Energy Fuel* 23, 2832 (2009).
23. P.G. Loutzenhiser and A. Steinfeld, *Int. J. Hydrogen Energy* 36, 12141 (2011).
24. A. Stamatiou, P.G. Loutzenhiser, and A. Steinfeld, *Chem. Mater.* 22, 851 (2010).
25. J. Petrasch, P. Coray, A. Meier, M. Brack, P. Häberling, D. Wuillemin, and A. Steinfeld, *J. Sol. Energy-Trans. ASME* 129, 405 (2007).
26. W.T. Welford and R. Winston, *High Collection Nonimaging Optics* (San Diego, CA: Academic Press, 1989).
27. A. Yogev, M. Epstein, and A. Kogan, *Int. J. Hydrogen Energy* 23, 239 (1998).
28. C. Wieckert, A. Meier, and A. Steinfeld, *J. Sol. Energy-Trans. ASME* 125, 120 (2003).
29. C. Wieckert, *J. Sol. Energy-Trans. ASME* 127, 425 (2005).
30. S. Steinlechner, *Waelz Oxide Characterization*, unpublished report for Befesa (Leoben, Austria: Department of Metallurgy, Montan University, 2012).
31. S. Kräupl, U. Frommherz, and C. Wieckert, *J. Sol. Energy-Trans. ASME* 128, 8 (2006).
32. G. Graf, *Ullmann's Encyclopedia of Industrial Chemistry*, Vol. A28 (Weinheim, Germany: VCH Verlagsgesellschaft, 1996), pp. 509–530.